SLAC-PUB-7101
January 1996

SPIN STRUCTURE MEASUREMENTS FROM E143 AT SLAC*

Linda M. Stuart
Stanford Linear Accelerator Center
Stanford University, Stanford, California 94309

Representing the E143 Collaborations

Abstract

Measurements were made of the proton and deuteron spin structure functions g_1^p and g_1^d at beam energies of 29.1, 16.2, and 9.7 GeV, and g_2^p and g_2^d at a beam energy of 29.1 GeV. The integrals $\Gamma_p = \int_0^1 g_1^p(x,Q^2)dx$ and $\Gamma_d = \int_0^1 g_1^d(x,Q^2)dx$ were evaluated at fixed $Q^2 = 3$ (GeV/c)^2 using the 29.1 GeV data to yield $\Gamma_p = 0.127 \pm 0.004$(stat.) $\pm$ 0.010(syst.) and $\Gamma_d = 0.041 \pm 0.003 \pm 0.004$. The Q^2 dependence of the ratio g_1/F_1 was studied and found to be small for $Q^2 > 1$ (GeV/c)^2. Within experimental precision the g_2 data are well-described by the twist-2 contribution, g_2^{WW}. Twist-3 matrix elements were extracted and compared to theoretical predictions. The asymmetry A_2 was measured and found to be significantly smaller than the positivity limit $\sqrt{R}$ for both proton and deuteron targets. A_2^p is found to be positive and inconsistent with zero.

Presented at the XXIII SLAC Summer Institute on Particle Physics Topical Conference, Stanford University, Stanford CA, July 19–21, 1995

*Work supported in part by Department of Energy contract DE–AC03–76SF00515.

1 Introduction

Measurements of nucleon spin-dependent structure functions are valuable tools used to understand the complex nature of nucleon structure. These structure functions are probes of the longitudinal and transverse quark and gluon polarization distributions inside the nucleons. Measurements of these structure functions allow us to test sum rules, quark-model predictions, and QCD predictions.

The spin-dependent structure functions $g_1(x,Q^2)$ and $g_2(x,Q^2)$ are measured by scattering longitudinally polarized leptons from a target that is polarized either longitudinally or transversely. The longitudinal ($A_{||}$) and transverse ($A_{\perp}$) asymmetries are formed from combining data taken with opposite beam helicity, and the structure functions are determined from these asymmetries:

$$\begin{aligned} g_1(x,Q^2) &= \frac{F_1(x,Q^2)}{d}\ [A_{||} + \tan(\theta/2)A_{\perp}]\ , \\ g_2(x,Q^2) &= \frac{yF_1(x,Q^2)}{2d}\quad \left[\frac{E+E'\cos\theta}{E'\sin\theta}A_{\perp} - A_{||}\right]\ , \end{aligned} \tag{1}$$

where E is the incident electron energy, E' is the scattered electron energy, θ is the scattering angle, x is the Bjorken scaling variable, Q^2 is the four-momentum transfer squared, $y = (E-E')/E$, $d = [(1-\epsilon)(2-y)]/[y(1+\epsilon R(x,Q^2))]$, $\epsilon^{-1} = 1 + 2[1+\gamma^{-2}]\tan^2(\theta/2)$, $\gamma = 2Mx/\sqrt{Q^2}$, M is the nucleon mass, $F_1(x,Q^2)$ is one of the spin-averaged structure functions, and $R(x,Q^2) = \sigma_L/\sigma_T$ is the ratio of longitudinal and transverse virtual photon-absorption cross sections. Also of interest are the virtual photon-absorption asymmetries

$$A_1 = \frac{\sigma_{1/2} - \sigma_{3/2}}{\sigma_{1/2} + \sigma_{3/2}}\ , \qquad \text{and} \qquad A_2 = \frac{2\sigma_{TL}}{\sigma_{1/2} + \sigma_{3/2}}\ , \tag{2}$$

where $\sigma_{1/2}$ and $\sigma_{3/2}$ are the virtual photon-nucleon absorption cross sections for total helicity between photon and nucleon of 1/2 and 3/2 respectively,

and σ_{TL} is an interference term between the transverse and longitudinal photon-nucleon amplitudes. These asymmetries are also determined from the measured asymmetries:

$$A_1 = \frac{1}{d}\left[A_{\|}(1+xM/E) - A_{\perp}\frac{xM}{E\tan(\theta/2)}\right],$$
$$A_2 = \frac{\gamma(2-y)}{2d}\left[A_{\perp}\frac{y(1+xM/E)}{(1-y)\sin\theta} + A_{\|}\right]. \quad (3)$$

1.1 Physical Interpretation of g_1

The structure function $g_1(x)$ is interpreted in the naive parton model as the charge weighted difference between momentum distributions for quarks and nucleon helicities aligned parallel ($\uparrow$) and antiparallel ($\downarrow$):

$$g_1(x) = \frac{1}{2}\sum_i e_i^2[q_i^{\uparrow}(x) - q_i^{\downarrow}(x)] \equiv \sum_i e_i^2 \Delta q_i(x)\ , \quad (4)$$

where e_i is the charge of quark flavors i, and $q_i^{\uparrow(\downarrow)}(x)$ are the quark plus antiquark momentum distributions. The quantity $\int_0^1 \Delta q_i(x)dx = \Delta i$ refers to the helicity of quark species $i = u, d, s$ in the proton, and $\Delta q = \Delta u + \Delta d + \Delta s$ is the net helicity of quarks. Using measurements of $\int_0^1 g_1(x)dx$, g_A/g_V and F/D, as well as the QCD corrections to the sum rules, one can separately extract the quantities Δ_i.[1]

1.2 Physical Interpretation of g_2

Unlike g_1, the interpretation of g_2 in the naive parton model is ambiguous.[2] A more advanced light-cone parton model,[3,4] as well as an operator product expansion (OPE) analysis,[5] indicate that there are three components contributing to g_2. These components include the leading twist-2 part $g_2^{WW}(x, Q^2)$, coming from the same set of operators that contribute to g_1, another twist-2 part coming

from the quark transverse-polarization distribution $h_T(x,Q^2)$, and a twist-3 part coming from quark-gluon interactions $\xi(x,Q^2)$:

$$g_2(x,Q^2) = g_2^{WW}(x,Q^2) - \int_x^1 \frac{\partial}{\partial y}\left(\frac{m}{M}h_T(y,Q^2) + \xi(y,Q^2)\right)\frac{dy}{y} \ . \qquad (5)$$

The quark mass is denoted by m, and the g_2^{WW} expression of Wandzura-Wilczek[6] is given by

$$g_2^{WW}(x,Q^2) = -g_1(x,Q^2) + \int_x^1 \frac{g_1(y,Q^2)}{y}\,dy \ . \qquad (6)$$

2 Sum Rules

2.1 Bjorken Sum Rule

A sum rule developed by Bjorken[7] relates the integral over the proton minus neutron spin structure functions to the nucleon beta decay weak coupling constants. It is believed to be strictly valid at infinite Q^2:

$$\int (g_1^p(x) - g_1^n(x))\,dx \ = \ \frac{1}{6}\,\frac{g_A}{g_V} \ , \qquad Q^2 = \infty \ , \qquad (7)$$

where g_A and g_V are the nucleon axial-vector and vector coupling constants, and $g_A/g_V \ = \ 1.2573 \pm 0.0038$.[8] The advent of QCD corrections has brought this sum rule into the regime where it (and thus the QCD corrections) can be experimentally tested. The nonsinglet correction[9] to order three for three quark flavors is $C_{NS} \ = \ \left[1 - \alpha_s/\pi - 3.58\,(\alpha_s/\pi)^2 - 20.22\,(\alpha_s/\pi)^3\right]$ where $\alpha_s(Q^2)$ is the strong coupling constant.

2.2 Ellis-Jaffe Sum Rule

Other sum rules of interest for g_1, although less rigorous than the Bjorken sum rule, are the Ellis-Jaffe sum rules[10] which were derived using SU(3) symmetry and assuming the strange sea in the nucleons is unpolarized.

$$\Gamma_1^p(Q^2) \ = \ \int_0^1 g_1^p(x,Q^2)dx = \frac{1}{18}\left[C_{NS}(3F+D) + 2C_S(3F-D)\right] \ ,$$

$$\Gamma_1^n(Q^2) \;=\; \int_0^1 g_1^n(x,Q^2)dx = \frac{1}{9}\left[-DC_{NS} + C_S(3F-D)\right] \;, \tag{8}$$

where F and D are weak hyperon decay constants extracted from data[11] $F/D = 0.575 \pm 0.016$, $F + D = g_A/g_V$, and the second-order singlet QCD correction[12] is given by $C_S = \left[1 - 0.3333\alpha_s/\pi - 0.5495\,(\alpha_s/\pi)^2\right]$.

2.3 OPE Sum Rules

The OPE[2,5,13] is a useful technique within QCD because it separates the physics into a perturbative part that is easily treatable and a nonperturbative part that is parameterized in terms of unknown matrix elements of Lorentz-covariant operators. The OPE analysis of g_1 and g_2 yields an infinite number of sum rules:

$$\begin{aligned} \int_0^1 x^n\, g_1(x,Q^2)\, dx \;&=\; \frac{a_n}{2} \;, & n = 0,2,4,\ldots \;, \\ \int_0^1 x^n\, g_2(x,Q^2)\, dx \;&=\; \frac{1}{2}\,\frac{n}{n+1}\,(d_n - a_n) \;, & n = 2,4,\ldots \;, \end{aligned} \tag{9}$$

where a_n are the twist-2 and d_n are the twist-3 matrix elements of the renormalized operators. The OPE only gives information on the odd moments of the spin structure functions. The Wandzura-Wilczek relation in Eq. (6) can be derived from these sum rules by setting $d_n = 0$.

2.4 Burkhardt-Cottingham Sum Rule

The Burkhardt-Cottingham sum rule[14] for g_2 at large Q^2,

$$\int_0^1 g_2(x)dx = 0 \;, \tag{10}$$

was derived from from virtual Compton scattering dispersion relations. This sum rule does not follow from the OPE, since the $n = 0$ sum rule is not defined for g_2 in Eq. (9). The Burkhardt-Cottingham sum rule relies on g_2 obeying Regge theory, which may not be a good assumption. A non-Regge divergence of g_2 at low x would invalidate this sum rule,[2,5] and such a divergence could be very difficult to detect experimentally.

2.5 Efremov-Teryaev Sum Rule

The Efremov-Teryaev sum rule[15] is derived in leading order QCD where quark-gluon correlators have been included. This sum rule relates the g_1 and g_2 structure functions:

$$\int_0^1 x[2g_2(x) + g_1(x)]dx = 0 \ .$$

3 Other Experiments

The earliest spin structure experiments, E80,[16] E130,[17] and EMC,[18] measured $A_{||}$ for the proton only. Using the assumption that $g_1 \simeq F_1 A_1$, the EMC extracted $g_1^p(x, Q^2)$ with sufficient precision to test the Ellis-Jaffe sum rule (which was violated) and the so-called "spin crisis" was born. In the naive quark model, this was interpreted to mean that the total quark helicity was small and consistent with zero, while the strange quark helicity was negative and inconsistent with zero. This unexpected result has generated a lot of interest in the physics community. Many theoretical papers have surfaced to explain the data, and better QCD corrections have been calculated to bring predictions closer to experimental results. There are now extensive experimental programs at SLAC, CERN and HERA for learning more about nucleon spin structure. Results are now available from the SMC[19–22] experiment at CERN and the E142[23] experiment at SLAC. These data include significantly more-precise proton data, measurements on deuterons and ^{3}He (neutrons), and the first measurement of the transverse asymmetry A_2 for the proton. These experiments confirm the Bjorken sum rule, and show that the Ellis-Jaffe sum rules for both the proton and neutron are violated.

4 Experiment E143

For experiment E143,[24-27] longitudinally polarized electrons were scattered from polarized protons and deuterons into two independent spectrometers at angles of 4.5° and 7°. The beam polarization, typically $P_b = 0.85 \pm 0.02$, was measured with a Møller polarimeter. Measurements were made at three beam energies, 29.1, 16.2, and 9.7 GeV. The target cells were filled with granules of either $^{15}NH_3$ or $^{15}ND_3$, and were polarized using the technique of dynamic nuclear polarization. The targets can be polarized longitudinally or transversely relative to the beam by physically rotating the polarizing magnet. Target polarization P_t, measured by a calibrated NMR, averaged around 0.65 ± 0.017 for protons and 0.25 ± 0.011 for deuterons.

Experimental asymmetries $A_{||}$ and $A_\perp$ were determined from

$$A_{||} \text{ (or } A_\perp) = C_1\left(\frac{N_L - N_R}{N_L + N_R}\frac{1}{f P_b P_t} - C_2\right) + A_{RC} \ , \tag{11}$$

where N_L and N_R are the number of scattered electrons per incident electron for negative and positive beam helicity, with corrections made for charge-symmetric backgrounds and deadtime; f is the dilution factor representing the fraction of measured events originating from polarizable protons or deuterons within the target; C_1 and C_2 correct for the polarized nitrogen nuclei and for residual polarized protons in the ND_3 target; and A_{RC} are the radiative corrections, which include internal[28] and external[29] contributions.

4.1 Longitudinal results at $E = 29$ GeV

From the measured values of $A_{||}$ and $A_\perp$ we calculated the ratios g_1^p/F_1^p and g_1^d/F_1^d using the definition given in Eq. (1). For $F_1(x,Q^2) = F_2(x,Q^2)(1+\gamma^2)/[2x(1 + R(x,Q^2))]$ we used the NMC[30] fits to $F_2(x,Q^2)$ data and the SLAC fit[31] to

$R(x,Q^2)$, which was extrapolated to unmeasured regions for $x < 0.08$. These results[24,25] are shown in Fig. 1. Also included in the plots are the data from other experiments.[16–18,20,22] These data are all in good agreement with the E143 results.

Values of xg_1^p and xg_1^d at the average $Q^2 = 3$ (GeV/c)^2 of this experiment are shown in Fig. 2. The evaluation at constant Q^2 is model-dependent; we have made the assumption that g_1/F_1 is independent of Q^2, which is believed to be reasonable for the kinematics of this experiment (see discussion on Q^2 dependence below). Values of xg_1^p and xg_1^n from several experiments at an average $Q^2 = 5$ (GeV/c)^2 are shown in Fig. 3. The data were evolved to constant Q^2, assuming g_1/F_1 is independent of Q^2. The neutron results from this experiment[25] and from SMC[22] were extracted from proton and deuteron data using $g_1^d = \frac{1}{2}(g_1^p + g_1^n)(1 - \frac{3}{2}\omega_D)$, where ω_D is the probability that the deuteron is in a D state. Both experiments used $\omega_D = 0.05 \pm 0.01$.[8] We see from Fig. 3 that the data sets are in good agreement when evolved to the same Q^2.

The integrals over x of g_1 for the proton (Γ_1^p), deuteron (Γ_1^d), and neutron (Γ_1^n) were evaluated at a constant $Q^2 = 3$ (GeV/c)^2. The measured x region was $0.029 < x < 0.08$. The extrapolation from $x = 0.8$ to $x = 1$ was done assuming that g_1 varies as $(1-x)^3$ at high x. The extrapolation from $x = 0$ to $x = 0.029$ was determined by fitting the low-x data to a Regge[32] motivated form $g_1 = Cx^{-\alpha}$. An alternate form,[33] $g_1 = C\ln(1/x)$, which provides a good fit to the low-x F_2 data from NMC and HERA, gives consistent results within the uncertainties. Table 1 gives a summary of the measured and extrapolated contributions to Γ_1^p and Γ_1^d. Table 2 shows the E143 measurements for Γ_1^p, Γ_1^d, Γ_1^n and $\Gamma_1^p - \Gamma_1^n$, as well as the corresponding Ellis-Jaffe and Bjorken sum rule predictions for $Q^2 = 3$ (GeV/c)^2. The data consistently demonstrate that the Ellis-Jaffe sum rule is violated.

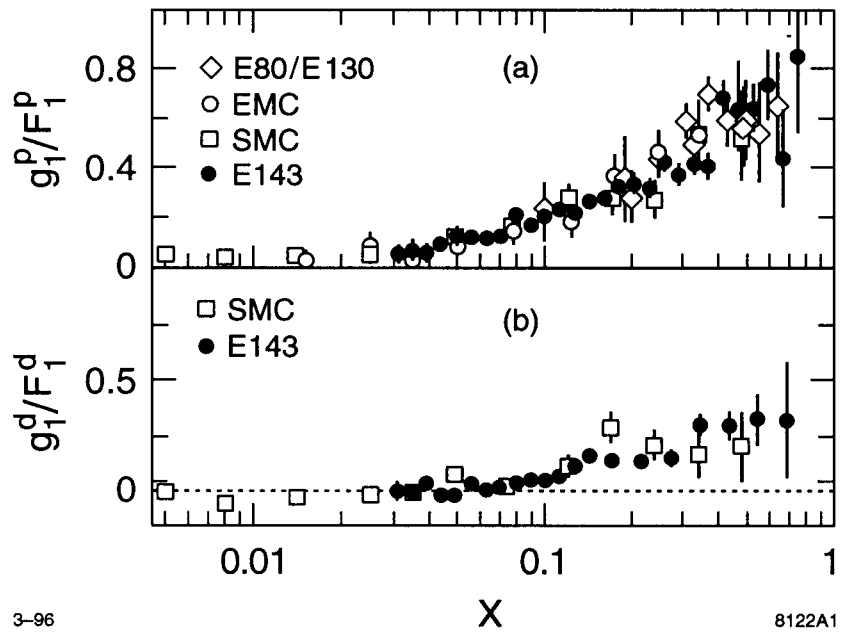

Figure 1: Measurements of g_1/F_1 for (a) proton and (b) deuteron for all experiments. The E143 data are in good agreement with all other data. The uncertainties for the E143 data include statistical contributions only.

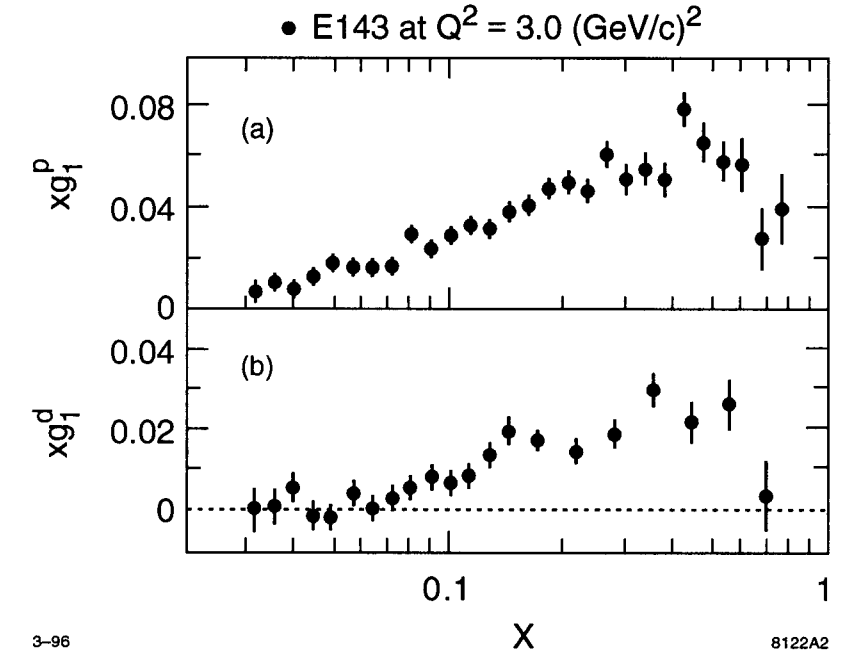

Figure 2: Measurements of xg_1 for (a) proton and (b) deuteron from experiment E143 at a constant $Q^2 = 3$ (GeV/c)^2. The uncertainties include statistical contributions only.

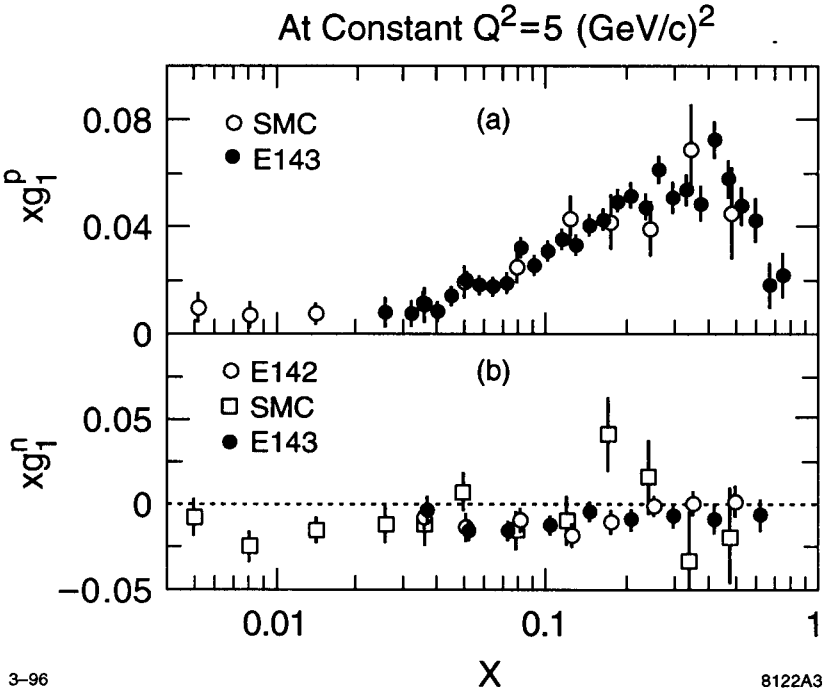

Figure 3: Measurements of xg_1 for (a) proton and (b) neutron for E143,[24,25] E142,[23] and SMC[20,22] at a constant $Q^2 = 5$ (GeV/c)^2. The data sets are in agreement. The uncertainties for the E143 data include statistical only.

Table 1: Results for Γ_1^p and Γ_1^d from experiment E143, broken up into the measured and extrapolated contributions. The measured contribution has a statistical and systematic uncertainty. The uncertainty on the extrapolated contributions is assumed to be systematic.

x Region	Γ_1^p	Γ_1^d
$0 < x < 0.029$	0.006 ± 0.006	0.001 ± 0.001
$0.029 < x < 0.8$	$0.120 \pm 0.004 \pm 0.008$	$0.040 \pm 0.003 \pm 0.004$
$0.8 < x < 1$	0.001 ± 0.001	0.000 ± 0.001
Total	$0.127 \pm 0.004 \pm 0.010$	$0.042 \pm 0.003 \pm 0.004$

Table 2: Summary of E143 g_1 sum rule results			
	Measured	Prediction	Sum Rule
Γ_p	$0.127 \pm 0.004 \pm 0.010$	0.160 ± 0.006	Ellis-Jaffe
Γ_d	$0.042 \pm 0.003 \pm 0.004$	0.069 ± 0.004	Ellis-Jaffe
Γ_n	$-0.037 \pm 0.008 \pm 0.011$	-0.011 ± 0.006	Ellis-Jaffe
$\Gamma_p - \Gamma_n$	$0.163 \pm 0.010 \pm 0.016$	0.171 ± 0.008	Bjorken

Table 3: Summary of the systematic errors contributing to the E143 g_1 integrals.				
Source	Γ_p	Γ_d	Γ_n	Γ_p-Γ_n
Beam polarization	0.003	0.001	0.001	0.004
Target polarization	0.003	0.002	0.005	0.007
Dilution factor	0.004	0.002	0.006	0.008
Radiative corrections	0.002	0.002	0.006	0.007
F_2, R	0.004	0.001	0.002	0.005
Extrapolation	0.006	0.001	0.004	0.006
Total	0.010	0.004	0.011	0.016

The most precise determination is given by the deuteron measurement, which is more than 3 σ away from the prediction. Note that the E143 results agree with the E142 results[23] for $\Gamma_1^n = -0.022 \pm 0.011$ at $Q^2 = 2$ (GeV/c)^2, and the SMC[20,22] results for $\Gamma_1^p = 0.136 \pm 0.016$ and $\Gamma_1^d = 0.034 \pm 0.011$ at $Q^2 = 10$ (GeV/c)^2. The estimated Q^2 dependence of these quantities for $2 < Q^2 < 10$ (GeV/c)^2 is within the errors on all the experiments. Table 3 is a summary of the dominant systematic errors contributing to the E143 measured integrals shown in Table 2.

Violation of the Ellis-Jaffe sum rule may imply that the assumption that the strange quark is unpolarized within the nucleon is false. This can be seen by extracting the net quark helicity within the proton using the naive quark model[1] (See Eq. (4) and related discussion). Table 4 gives the extracted quark helicities, as determined from the measurements of Γ_1^p and Γ_1^d and the SU(3) coupling constants F and D. The data include third-order nonsinglet and second-order singlet QCD

corrections. The net quark helicity Δq is significantly less than a prediction[10] that $\Delta q = 0.58$, assuming zero strange quark helicity and SU(3) flavor symmetry in the baryon octet. Also, Δs is negative and significantly different from zero. Figure 4 shows a plot of Δq versus Δs, as extracted from various experimental measurements at the appropriate Q^2. We see that all experiments are consistent with a small Δq, and a Δs that is negative and inconsistent with zero.

Table 4: Extracted quark helicities from experiment E143.

	Γ_p	Γ_d
Δu	0.81 ± 0.04	0.83 ± 0.02
Δd	-0.44 ± 0.04	-0.43 ± 0.02
Δs	-0.10 ± 0.04	-0.09 ± 0.02
Δq	0.27 ± 0.11	0.30 ± 0.06

4.2 Transverse results at $E = 29$ GeV

From the measured values of $A_{\|}$ and $A_{\perp}$ at $E = 29$ GeV, we calculated g_2^p, g_2^d, A_2^p, and A_2^d, using Eqs. (1) and (3). The results for A_2 for the proton and deuteron are shown in Fig. 5. The systematic errors, dominated by radiative correction uncertainties, are indicated by bands for the two spectrometers used in the experiment. The data agree within errors, despite the differences in Q^2 of the measurements (nearly a factor of two). Figure 5 also shows the proton results from SMC,[21] and the $\sqrt{R}$ positivity limits[31] for each data set. The data are much closer to zero than the positivity limit. Results for A_2^p are consistently > 0, and since A_2 is expected to be zero at high Q^2 because $R \to 0$, these data indicate that A_2 must have Q^2 dependence. A comparison of the data with the hypothesis $A_2 = 0$ yields $\chi^2 = 73$ for the proton and $\chi^2 = 44$ for the deuteron for 48 degrees of freedom.

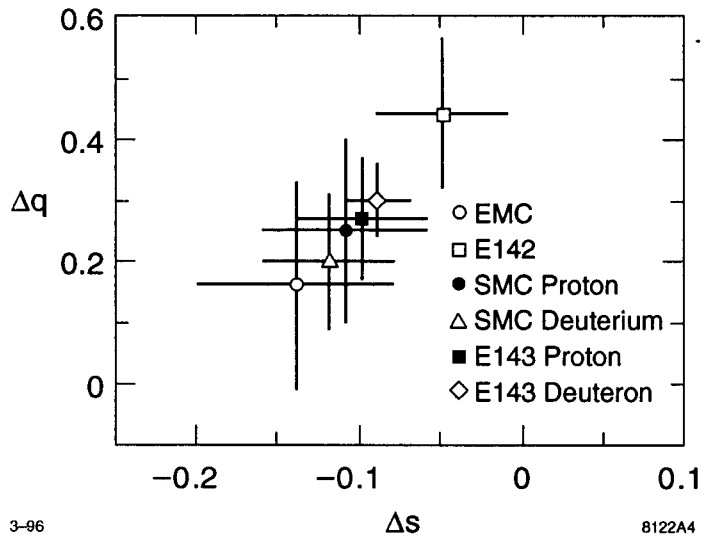

Figure 4: The quark helicity content of the proton as extracted from various measurements is shown for Δq versus Δs. The data include third-order nonsinglet and second-order singlet QCD corrections.

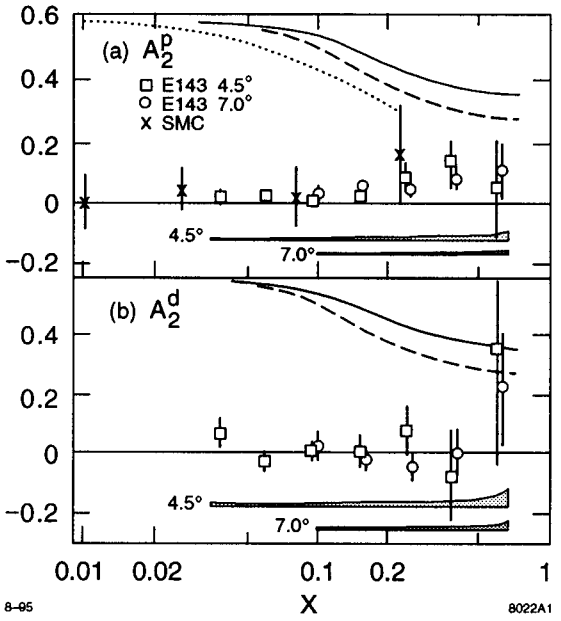

Figure 5: Measurements of (a) A_2^p, and (b) A_2^d from E143[26] and SMC.[21] Systematic errors are indicated by bands. The curves show the $\sqrt{R}$[31] positivity constraints for the three data sets. The solid, dashed, and dotted curves correspond to the 4.5° E143, 7.0° E143, and SMC kinematics, respectively. Overlapping data have been shifted slightly in x to make errors clearly visible.

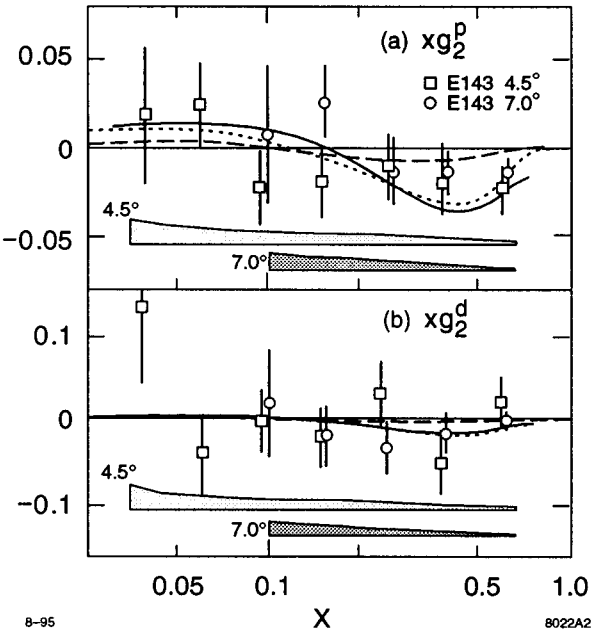

Figure 6: Spin structure function measurements for (a) xg_2^p, and (b) xg_2^d from E143. Systematic errors are indicated by bands. Overlapping data were shifted slightly in x to make errors clearly visible. The solid curve shows the twist-2 g_2^{WW} calculation for the kinematics of the 4.5° spectrometer. The same curve for 7° is nearly indistinguishable. Bag-model calculations at $Q^2 = 5.0$ (GeV/c)^2 by Stratmann[34] (dotted) and Song and McCarthy[35] (dashed) are indicated.

The results for xg_2 for the proton and deuteron are shown in Fig. 6. The g_2^d results are per nucleon. The systematic errors are indicated by bands. Also shown is the g_2^{WW} curve evaluated using Eq. (6) at $E = 29$ GeV and $\theta = 4.5°$. The same curve for $\theta = 7°$ is nearly indistinguishable. The values for g_2^{WW} were determined from $g_1(x, Q^2)$ evaluated from a fit to world data of A_1[27] and assuming negligible higher-twist contributions. Also shown are the bag-model predictions of Stratmann[34] and Song and McCarthy,[35] which include both twist-2 and twist-3 contributions for $Q^2 = 5$ (GeV/c)^2. At high x, the results for g_2^p indicate a negative trend consistent with the expectations for g_2^{WW}. The deuteron results are less conclusive because of the larger errors.

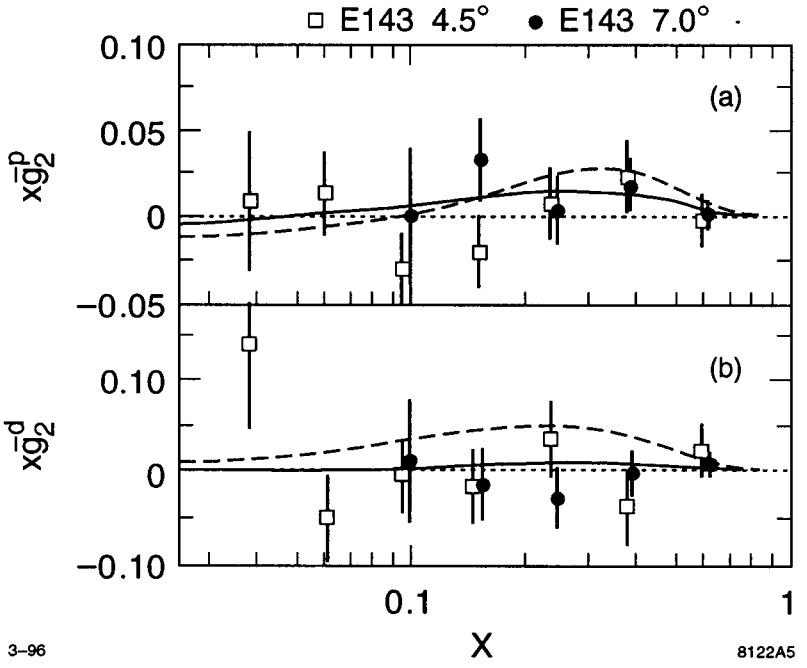

Figure 7: E143 results[26] for (a) $x\overline{g_2}^p$, and (b) $x\overline{g_2}^d$ Overlapping data have been shifted slightly in x to make errors clearly visible. Bag-model calculations at $Q^2 = 5.0$ (GeV/c)^2 by Stratmann[34] (solid) and Song and McCarthy[35] (dashed) are indicated.

We can look for possible quark-mass and higher-twist effects by extracting the quantity $\overline{g_2}(x,Q^2) = g_2(x,Q^2) - g_2^{WW}(x,Q^2)$, If the term in Eq. (5) which depends on quark masses can be neglected, then $\overline{g_2}(x,Q^2)$ is entirely twist-3. Our results can be seen in Fig. 7. Within the experimental uncertainty, the data are consistent with $\overline{g_2}$ being zero but also with $\overline{g_2}$ being of the same order of magnitude as g_2^{WW}. Also shown in Fig. 7 are the bag-model predictions of Stratmann[34] and Song and McCarthy[35] for $Q^2 = 5$ (GeV/c)^2, which compare favorably with the data, given the large experimental uncertainties.

Using our results for the longitudinal spin structure functions g_1^p and g_1^d, we computed the first few moments of the OPE sum rules and solved for the twist-3 matrix elements d_n. These moments are defined to be $\Gamma_1^{(n)} = \int_0^1 x^n g_1(x)dx$ and $\Gamma_2^{(n)} = \int_0^1 x^n g_2(x)dx$. For the measured region $0.03 < x < 0.8$, we

evaluated g_1 and corrected the twist-2 part of g_2 to fixed $Q^2 = 5$ (GeV/c)^2, assuming g_1/F_1 is independent of Q^2, and averaged the two spectrometer results to evaluate the moments. Possible Q^2 dependence of $\overline{g_2}$ has been neglected. We neglect the contribution from the region $0 \leq x < 0.03$ because of the x^n suppression factor. For $0.8 < x \leq 1$, we assume that both g_1 and g_2 behave as $(1-x)^3$, and we fit the data for $x > 0.56$. The uncertainty in the extrapolated contribution is taken to be the same as the contribution.

Table 5a: Results for the moments $\Gamma_1^{(n)}$ and $\Gamma_2^{(n)}$ evaluated at $Q^2 = 5$ (GeV/c)^2, and the extracted twist-3 matrix elements d_n for proton (p) and deuteron (d) targets. The errors include statistical (which dominate) and systematic contributions.

	n	$\Gamma_1^{(n)}$	$\Gamma_2^{(n)}$	d_n
p	2	0.0121 ± 0.0010	-0.0063 ± 0.0018	0.0054 ± 0.0050
	4	0.0032 ± 0.0004	-0.0023 ± 0.0006	0.0007 ± 0.0017
	6	0.0012 ± 0.0002	-0.0010 ± 0.0003	0.0001 ± 0.0008
d	2	0.0040 ± 0.0008	-0.0014 ± 0.0030	0.0039 ± 0.0092
	4	0.0008 ± 0.0003	0.0000 ± 0.0010	0.0017 ± 0.0026
	6	0.0002 ± 0.0001	0.0001 ± 0.0005	0.0006 ± 0.0011

Table 5b: Theoretical predictions for the twist-3 matrix element d_2^p for proton and d_2^d for deuteron. The values for Q^2 are in (GeV/c)^2.

	Bag models		QCD sum rules	
	Ref. [35]	Ref. [34]	Ref. [36]	Ref. [37]
Q^2	5	5	1	1
d_2^p	0.0176	0.0060	-0.006 ± 0.003	-0.003 ± 0.006
d_2^d	0.0066	0.0029	-0.017 ± 0.005	-0.014 ± 0.006

The results are shown in Table 5a. For comparison, in Table 5b we quote theoretical predictions[34-37] for d_2^p and d_2^d. For d_2^d, the proton and neutron results were averaged, and a deuteron D-state correction was applied. Our extracted

values for d_n are consistent with zero, but the errors are large. These results do not have sufficient precision to distinguish between the model predictions.

We also evaluated the integrals $\int_{0.03}^{1} g_2(x)dx$ and $\int_{0.03}^{1} x[2g_2(x) + g_1(x)]dx$ for both the proton and deuteron structure functions. We do not attempt a low-x extrapolation due to the theoretical uncertainty on the low-x behavior of g_2. For the latter integral, the low-x region is suppressed by x, so it is not unreasonable to assume that the low-x extrapolation is negligible. The high-x extrapolation is done as discussed above. The results are given in Table 6, and are all consistent with zero within their large errors, as expected from the Burkhardt-Cottingham and Efremov-Teryaev sum rules. Of course, we cannot really test the Burkhardt-Cottingham sum rule, due to the uncertainty in the unmeasured low-x behavior.

Table 6: Summary of E143 g_2 sum rule results. The predictions for both sum rules are zero.

	$\int_{0.03}^{1} g_2(x)dx$	$\int_{0.03}^{1} x[2g_2(x) + g_1(x)]dx$
Proton	-0.013 ± 0.028	0.008 ± 0.008
Deuteron	-0.033 ± 0.082	-0.001 ± 0.014

4.3 Q^2 Dependence of g_1

Data for g_1 measured at a fixed energy of 29 GeV were discussed above. These data cover the range $1 < Q^2 < 10$ (GeV/c)^2 where the lower values of Q^2 are at the lower values of x. In order to evaluate sum rules at some fixed Q^2, it is necessary to extrapolate the data from the measured kinematics. Since this is a model-dependent procedure (e.g., assuming g_1/F_1 is independent of Q^2), it is useful to measure the Q^2 dependence by taking data at multiple beam energies. In experiment E143, we made measurements at beam energies of 29.1, 16.2, and 9.7 GeV. The kinematic coverage of these data sets, where a Q^2-dependent measurement has been made, is $0.03 < x < 0.6$ and $0.3 < Q^2 < 10$ (GeV/c)^2.

According to the GLAP equations,[38] which give the predicted Q^2 dependence of the nucleon polarized and unpolarized quark and gluon distribution functions, g_1 is expected to evolve logarithmically in a way similar to the unpolarized structure functions $F_1(x,Q^2)$ and $F_2(x,Q^2)$. The Q^2 dependence of the ratio g_1/F_1 may be independent of Q^2 to a first approximation, but the precise behavior is sensitive to the underlying spin-dependent quark and gluon distribution functions. Futher measurements will help pin down this behavior. Fits have been made[39,40] of $g_1(x,Q^2)$ data using next-to-leading-order (NLO) GLAP equations.[41] The results indicate that NLO fits are more sensitive to the strength of the polarized gluon distribution function $\Delta G(x,Q^2)$ than previous leading-order (LO) fits.[41–45] In addition our understanding of the Q^2 dependence of g_1 is complicated by possible higher-twist contributions that are not part of the GLAP equations. These terms are expected to behave as $C(x)/Q^2$, $D(x)/Q^4$, etc., where $C(x)$ and $D(x)$ are unknown functions.

The ratio g_1/F_1 has been extracted from the data taken in this experiment,[27] as well as from other available data for the proton[16–18,20] and the deuteron,[22] using the relations given in Eq. (1). The twist-2 model of Wandzura and Wilczek[6] given in Eq. (6) was used to describe g_2 for all data, since the E143 g_2 data discussed above are in agreement with this model. The results for g_1^p/F_1^p and g_1^d/F_1^d are shown in Figs. 8 and 9, respectively, for eight values of x. Improved radiative corrections were applied to the E80[16] and E130[17] results. Only statistical uncertainties are shown. For the present experiment, most systematic uncertainties (beam polarization, target polarization, fraction of polarizable nucleons in the target) for a given target are common to all data, corresponding to an overall normalization error of about 5% for the proton data and 6% for the deuteron data. The remaining point-to-point systematic uncertainties (radiative corrections, model uncertainties for $R(x,Q^2)$, resolution corrections) vary over x from a few percent to 15%, and

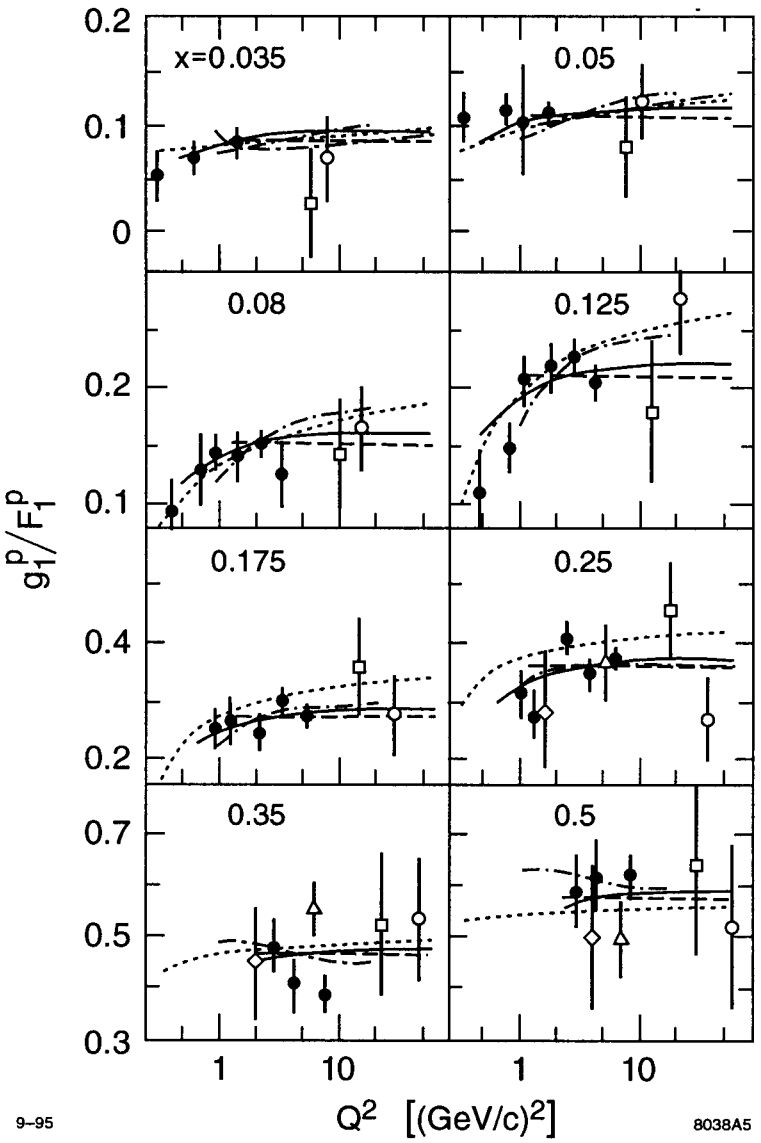

Figure 8: Ratios g_1^p/F_1^p extracted from experiments assuming $g_2 = g_2^{WW}$. The uncertainties are statistical only. Data are from E143[27] (solid circles), E80[16] (diamonds), E130[17] (triangles), EMC[18] (squares), and SMC[20] (open circles). The dashed and solid curves correspond to global fits[27] II (g_1^p/F_1^p Q^2-independent) and III (g_1^p/F_1^p Q^2-dependent), respectively. Representative NLO pQCD fits from Ref. [39] and Ref. [40] are shown as the dot-dashed and dotted curves, respectively.

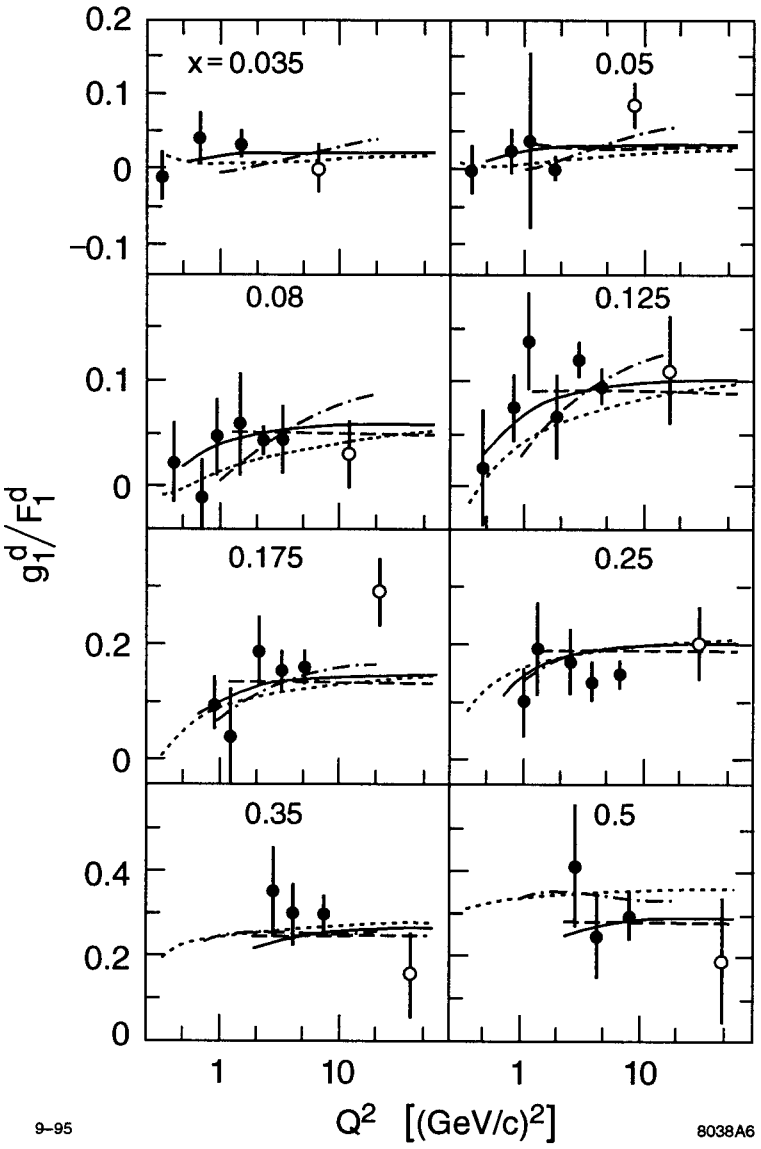

Figure 9: Ratios g_1^d/F_1^d from E143[27] (solid circles) and SMC[22] (open circles). The curves are as in Fig. 8.

are consistently less than the statistical uncertainties for all data. We see in Figs. 8 and 9 that g_1/F_1 is approximately independent of Q^2 at fixed x, although there is a noticeable trend for the ratio to decrease for $Q^2 < 1$ (GeV/c)^2.

We performed several simple global fits[27] to the data, in order to have a practical parameterization (needed, for example, in making radiative corrections to the data), and to study the possible Q^2 dependence of the first moments of g_1. The fits are of the general form $g_1/F_1 = ax^\alpha(1 + bx + cx^2)[1 + Cf(Q^2)]$, where a, α, b, c, and C are fit parameters, and $f(Q^2)$ is defined to be either $1/Q^2$ or $\ln(1/Q^2)$. Cuts were applied to some of the fits to include only data with $Q^2 > 1$ (GeV/c)^2, and C was forced to be zero (no Q^2 dependence) for some fits. The results indicate that when all the data are included, the fits where $C \neq 0$ have significantly better χ^2 per degree-of-freedom than those where $C = 0$. However, good fits to the data are obtained when $C = 0$ and the $Q^2 > 1$ (GeV/c)^2 cut is applied to the data (fit II). Two of these global fits,[27] fit II (described above) and fit III ($f(Q^2) = 1/Q^2$, and data at all Q^2 are fit) are shown in both Figs. 8 and 9.

Also shown in Figs. 8 and 9 are representative global NLO pQCD fits[39,40] to available structure function data, excluding those measured at the 9.7 GeV and 16.2 GeV beam energies of this experiment. These fits are indicated as the dot-dashed curves[39] and the dotted curves.[40] Both sets of predictions[39,40] indicate that g_1^p/F_1^p decreases with Q^2 at lower x, in agreement with the trend of our $E = 9.7$ and $E = 16.2$ results.

Another type of fit was made to the data, motivated by possible differences in the twist-4 contributions to g_1 and F_1. We fit the data in each x bin (see Figs. 8 and 9) with the form $g_1/F_1 = a(1 + C/Q^2)$. The results for the C coefficients are shown in Fig. 10 for fits to all data (circles) and for fits to data with $Q^2 > 1$ (GeV/c)^2 (squares). The coefficients indicate significantly negative values for C at intermediate values of x when all the data are fit. The errors are much larger

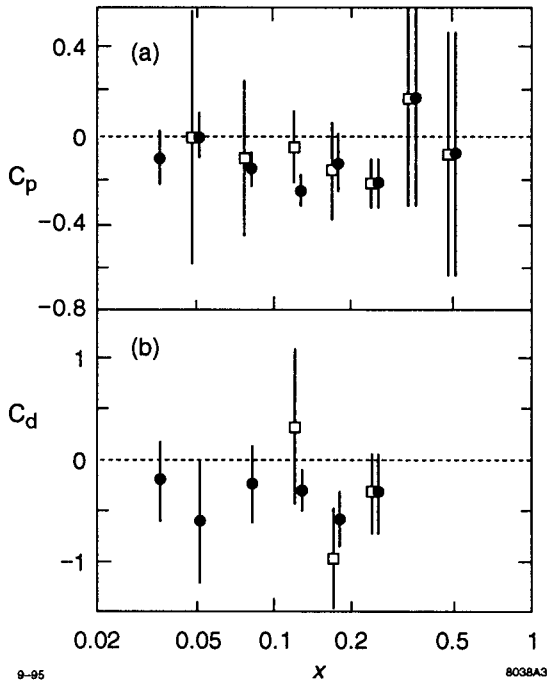

Figure 10: Coefficients C for fits to g_1/F_1 at fixed x of the form $a(1 + C/Q^2)$ for (a) proton and (b) deuteron. Solid circles are from fits to all data, and open squares are from fits to data with $Q^2 > 1$ (GeV/c)^2 only.

when data with $Q^2 < 1$ (GeV/c)^2 are excluded, and the results are consistent with no Q^2-dependence to g_1/F_1 ($C = 0$). The present data do not have sufficient precision to distinguish between a logarithmic and power-law Q^2 dependence, but can rule out large differences between the Q^2 dependence of g_1 and F_1, especially for $Q^2 > 1$ (GeV/c)^2.

Using fits[27] II and III described above, and a global fit[30,31] to F_1, we have evaluated the first moments Γ_1^p and Γ_1^d, and the corresponding results for $\Gamma_1^p - \Gamma_1^n$ and the net quark helicity Δq. The results for $\Gamma_1^p - \Gamma_1^n$ are shown as a function of Q^2 as the lower (fit II) and upper (fit III) bands in Fig. 11, where the width of the band reflects the combined statistical and systematic error estimate. Both fits are in reasonable agreement with the Bjorken sum rule (solid curve) evaluated using $\alpha_s(Q^2)$ evolved in Q^2 from $\alpha_s(M_Z) = 0.117 \pm 0.005$[8] for the QCD corrections.

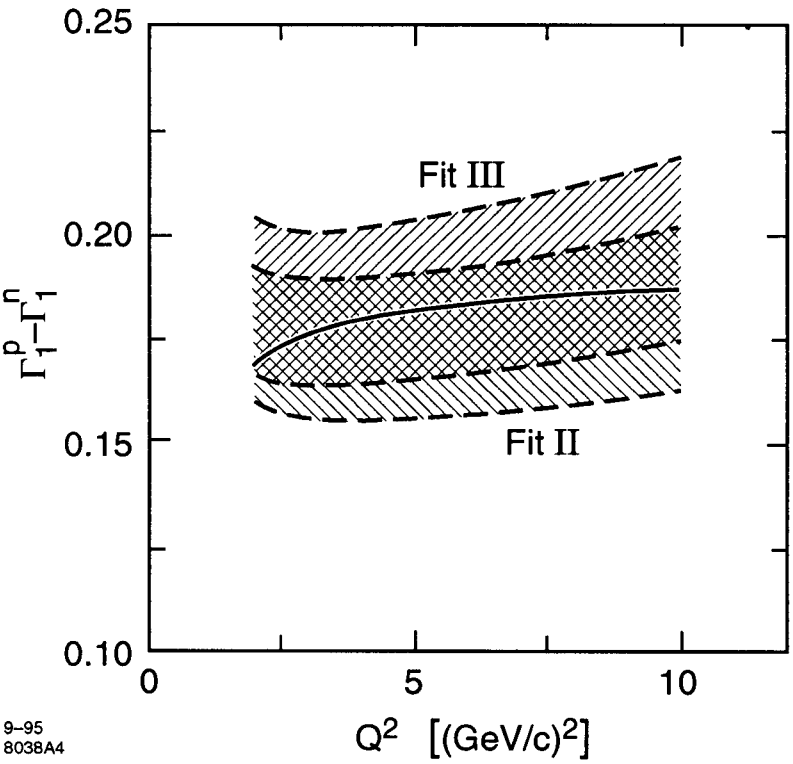

Figure 11: Evaluations of $\Gamma_1^p - \Gamma_1^n$ from the Q^2-independent fits II (lower band) and Q^2-dependent fits III (upper band). The errors include both statistical and systematic contribution, and are indicated by the widths of the bands. The solid curve is the prediction of the Bjorken sum rule with third-order QCD corrections.

Table 7: Summary of extracted Δq results at $Q^2 = 3$ (GeV/c)^2 using fits II and III[27] for Γ_p and Γ_d.

Fit	Δq from Γ_p	Δq from Γ_d
II (Q^2-independent)	0.34 ± 0.09	0.35 ± 0.05
III (Q^2-dependent)	0.36 ± 0.10	0.34 ± 0.05

Our results for Δq evaluated at $Q^2 = 3$ (GeV/c)^2 are shown in Table 7. Note that these results for Δq and for $\Gamma_1^p - \Gamma_1^n$ have shifted slightly from the original results[24,25] at 29 GeV discussed above (See Tables 2 and 4) because of improved radiative corrections, the inclusion of additional data runs, and improved measurements of the beam and target polarizations. Using fits II or III makes little

difference at $Q^2 = 3$ (GeV/c)^2, but we find Δq (which should be independent of Q^2) to vary less with Q^2 for fit III than for fit II, especially for the deuteron fits.

5 Summary

Measurements of $A_{\parallel}$ have been made at beam energies of 29.1, 16.2, and 9.7 GeV, and of $A_{\perp}$ at a beam energy of 29.1 GeV for protons and deuterons. The spin structure functions g_1 and g_2 have been extracted for the 29.1 GeV data. The integrals $\Gamma_p = \int_0^1 g_1^p(x,Q^2)dx$ and $\Gamma_d = \int_0^1 g_1^d(x,Q^2)dx$ have been evaluated at fixed $Q^2 = 3$ (GeV/c)^2. These results support the Bjorken sum rule predictions, and thus an important test of QCD is passed. However, the Ellis-Jaffe sum rule predictions for the proton and deuteron are violated. In the context of the quark model, this implies that a non-negligible fraction of the proton helicity is carried by either strange quarks, gluons, or both, and that the net quark helicity is smaller than expected. The Q^2 dependence of the ratio g_1/F_1 was studied and found to be small for $Q^2 > 1$ (GeV/c)^2.

Within experimental precision, we find that the g_2 data are well-described by the twist-2 contribution, g_2^{WW}. Results for $\overline{g_2}$ are consistent with zero, although $\overline{g_2}$ about the same order of magnitude as g_2^{WW} are allowed within the statistical uncertainties. More precise data is needed in the future to provide a more stringent measurement of $\overline{g_2}$. Twist-3 OPE matrix elements were extracted from the moments of g_1 and g_2. These results have a different sign than the QCD sum rule predictions, although within errors these predictions cannot be ruled out. The asymmetry A_2 was also measured, and found to be significantly smaller than the positivity limit $\sqrt{R}$ for both targets. A_2^p was found to be positive and inconsistent with zero.

A number of experimental programs will produce new spin structure function measurements in the future. SMC is continuing to take data. Additional

results are expected from SLAC using a 50 GeV incident electron beam, where measurements of the neutron spin structure functions are in progress (E154), and proton and deuterium spin structure function measurements (E155) will be made in 1996. The HERMES collaboration at HERA is also currently measuring spin-dependent structure functions of the proton and neutron. Data from these experiments will improve our understanding of the nucleon spin structure, and should answer many questions that have arisen due to current experimental results.

References

[1] F. E. Close and R. G. Roberts, Phys. Lett. B316, 165 (1993).

[2] M. Anselmino, A. Efremov, and E. Leader, Phys. Reports **261**, 1 (1995).

[3] L. Mankiewicz and Z. Rysak, Phys. Rev. **D43**, 733 (1991).

[4] J. L. Cortes, B. Pire, and J. P. Ralston, Z. Phys. **C55**, 409 (1992).

[5] R. L. Jaffe and X. Ji, Phys. Rev. **D43**, 724 (1991).

[6] S. Wandzura and F. Wilczek, Phys. Lett. **B72**, 195 (1977).

[7] J. D. Bjorken, Phys Rev. **148** 1467 (1966); Phys. Rev. **D1** 1376 (1970).

[8] Particle Data Group, L. Montanet *et al.,* Phys Rev. **D50**, 1173 (1994).

[9] S. A. Larin and J. A. M. Vermaseren, Phys. Lett. **B259**, 345 (1991) and references therein.

[10] J. Ellis and R. Jaffe, Phys. Rev. **D9**, 1444 (1974); Phys. Rev. **D10**, 1669 (1974).

[11] F. E. Close and R. G. Roberts, Phys. Lett. **B316**, 165 (1993).

[12] S. A. Larin, Phys Lett. **B334**, 192 (1994).

[13] E. V. Shuryak and A. I. Vainshtein, Nucl. Phys. **B201**, 141 (1982).

[14] H. Burkhardt and W. N. Cottingham, Ann. Phys. **56**, 453 (1970).

[15] A. V. Efremov and O. V. Teryaev, Phys. Lett. **B200**, 363 (1988).

[16] E80, M. Alguard *et al.*, PhysRev. Lett. **37**, 1261 (1976); Phys. Rev. Lett. **41**, 70 (1978).

[17] E130, G. Baum *et al.*, Phys. Rev. Lett. **51**, 1135 (1983).

[18] EMC, J. Ashman *et al.*, Nucl. Phys. **B328**, 1 (1989).

[19] SMC, B. Adeva *et al.*, Phys. Lett. **B302**, 533 (1993).

[20] SMC, D. Adams *et al.*, Phys. Lett **B329**, 399 (1994).

[21] SMC, D. Adams *et al.*, Phys. Lett. **B336**, 125 (1994).

[22] SMC, D. Adams *et al.*, Phys. Rev. Lett. **B357**, 248 (1995).

[23] E142, P.L. Anthony *et al.*, Phys Rev. Lett. **71**, 959 (1993).

[24] E143, K. Abe *et al.*, Phys. Rev. Lett. **74**, 346 (1995).

[25] E143, K. Abe *et al.*, Phys. Rev. Lett. **75**, 25 (1995).

[26] E143 K. Abe *et al.*, SLAC–PUB–95–6982 (1995), submitted to Phys. Rev. Lett.

[27] E143 K. Abe *et al.,* SLAC–PUB–95–6997 (1995), accepted by Phys. Lett. B.

[28] T. V. Kukhto and N. M. Shumeiko, Nucl . Phys. **B219**, 412 (1983); I. V. Akusevich and N. M. Shumeiko, J. Phys. **G20**, 513 (1994).

[29] Y. S. Tsai, SLAC–PUB–848 (1971); Y. S. Tsai, Rev. Mod. Phys. **46**, 815 (1974).

[30] NMC, P. Amaudruz *et al.,* Phys. Lett. **B295**, 159 (1992).

[31] L. W. Whitlow *et al.,* Phys. Lett. **B250**, 193 (1990).

[32] R. L. Heimann, Nucl. Phys. **B64**, 429 (1973).

[33] S. D. Bass and P. V. Landshoff, Report DAMTP 94/50 (1994); F. E. Close and R. G. Roberts, Report RAL–94–071 (1994).

[34] M. Stratmann, Z. Phys. **C60**, 763 (1993), and private communication for values at $Q^2 = 5$ (GeV/c)^2.

[35] X. Song and J. S. McCarthy, Phys. Rev. **D49**, 3169 (1994); **D50**, 4718 (1994) (Erratum); and X. Song, INPP–UVA–95/04 (1995).

[36] E. Stein *et al.*, Phys. Lett. **B334**, 369 (1995).

[37] I. I. Balitsky, V. M. Braun, and A. V. Kolesnichenko, Phys. Lett. **B242**, 245 (1990); **B318**, 648 (1993) (Erratum).

[38] G. Altarelli and G. Parisi, Nucl. Phys. B126, 298 (1977); V. N. Gribov and L. N. Lipatov, Yad. Fiz. 15, 781 (1972), [Sov. J. Nucl. Phys. 15, 438 (1972)].

[39] R. D. Ball, S. Forte, and G. Ridolfi, Nucl. Phys. B444, 287 (1995); and CERN–TH/95–266 (1995).

[40] M. Glück, E. Reya, M. Stratmann, and W. Vogelsang, Report DO–TH-95/13 and RAL–TR–95–042 (August 1995).

[41] E. B. Zijlstra and W. L. van Neerven, NuclPhys. B417, 61 (1994); R. Mertig and W. L. van Neervan, Univ. Leiden INLO–PUB–6/95 and NIKHEF–H/95–031 (June 1995).

[42] S. J. Brodsky, M. Burkardt, and I. Schmidt, Nucl. Phys. B441, 197 (1995).

[43] G. Altarelli, P. Nason, and G. Ridolfi, Phys. Lett. B320, 152 (1994).

[44] T. Gehrmann and W. J. Stirling, Z. Phys. C65 , 461 (1995).

[45] B. Ehrnsperger and A. Schäfer, Report UFTP/370/1994.